AD-A154 406 ACTIVE AND PASSIVE REMOTE SENSING OF ICE(U) 1/1
MASSACHUSETTS INST OF TECH CAMBRIDGE RESEARCH LAB OF
ELECTRONICS J A KONG SEP 84 N00014-83-K-0258

UNCLASSIFIED F/G 8/12 NL

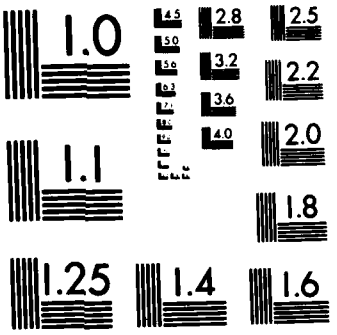

(2)

ACTIVE AND PASSIVE REMOTE SENSING OF ICE

Department of the Navy

Office of Naval Research

Contract N00014-83-K-0258

SEMI-ANNUAL REPORT

covering the period

February 1, 1984 – July 31, 1984

prepared by

J. A. Kong

September 1984

Massachusetts Institute of Technology
Research Laboratory of Electronics
Cambridge, Massachusetts 02139

Active and Passive Remote Sensing of Ice

Principal Investigator: Jin Au Kong

Semi-Annual Progress Report

This is a report on the progress that has been made in the study of active and passive remote sensing of ice ~~under the sponsorship of ONR Contract N00014-83-K-0258~~ during the period of February 1, 1984 - July 31, 1984. During this period we have: (1) calculated the emissivity of a two-layer anisotropic random medium; and (2) participated in the microwave sea ice measurement program at the Cold Regions Research and Engineering Laboratory (CRREL).

The emissivity of a two-layer anisotropic random medium has been calculated using the dyadic Green's function for a two-layer anisotropic medium and the first-order Born approximation. The emissivity is calculated by obtaining coherent and incoherent reflectivities and by making use of the relationship $e = 1 - r$. The incoherent reflectivity is obtained by integrating over the upper hemisphere the bistatic scattering coefficients obtained under the Born approximation. The theoretical results are illustrated by plotting the emissivities as functions of viewing angles and polarizations. They are used to interpret the passive microwave remote sensing data from vegetation canopy which also show strong anisotropic dependencies. Data obtained from the field measurements with corn stalks arranged in various configurations with perferred azimuthal directions are successfully interpreted with this model. It is expected that the radiometric data from CREEL measurements will also be successfully interpreted with this theoretical

model. A manuscript has been prepared for submission to a journal for publication [Appendix].

We have participated in the winter microwave remote sensing measurements at CRREL. Several trips were made to the experimental site at CRREL in order to assist and participate in the experimental efforts. Our involvement in the experimental efforts has provided us with valuable insights in the development of theoretical models and data interpretation.

Publications Sponsored by ONR

A. Refereed Journal Articles

1. J. K. Lee and J. A. Kong, "Dyadic Green's functions for layered anisotropic medium," **Electromagnetics**, **3**, 111-130, 1983.

2. J. K. Lee and J. A. Kong, "Active microwave remote sensing of layered anisotropic random medium," to be published.

3. J. K. Lee and J. A. Kong, "Passive microwave remote sensing of an anisotropic random medium layer," to be published.

B. Conference Articles

4. L. Tsang and J. A. Kong, "Scattering of electromagnetic waves from a half-space of densely distributed dielectric scatterers," **IEEE/APS Symposium and URSI Meeting**, Houston, Texas, May 23-26, 1983.

5. L. Tsang and J. A. Kong, "Theory of microwave remote sensing of dense medium," **IEEE/GRS Symposium and URSI Meeting**, San Francisco, September 1983.

6. Y. Q. Jin and J. A. Kong, "Wave scattering by a bounded layer of random discrete scatterers," **URSI Symposium**, Boulder, Colorado, January 11-14, 1984.

7. J. K. Lee and J. A. Kong, "Active and passive microwave remote sensing of layered anisotropic random medium," **URSI Symposium**, Boston, Mass., June 25-28, 1984.

C. Technical Reports

8. R. T. Shin and J. A. Kong, "Emissivity of a two-layer random medium with anisotropic correlation function," Technical Report No. EWT-RS-41-8303, MIT, 1983.

Appendix

PASSIVE MICROWAVE REMOTE SENSING OF AN ANISOTROPIC RANDOM MEDIUM LAYER

JAY KYOON LEE and JIN AU KONG

Department of Electrical Engineering and Computer Science and

Research Laboratory of Electronics

Massachusetts Institute of Technology

Cambridge, MA 02139

Abstract

The principle of reciprocity is invoked to calculate the brightness temperatures for passive microwave remote sensing of a two-layer anisotropic random medium. The bistatic scatttering coefficients are first computed with the Born approximation and then integrated over the upper hemisphere to be subtracted from unity, in order to obtain the emissivity for the random medium layer. The theoretical results are illustrated by plotting the emissivities as functions of viewing angles and polarizations. They are used to interpret remote sensing data obtained from vegetation canopy where the aniostropic random medium model applies. Field measurements with corn stalks arranged in various configurations with preferred azimuthal directions are successfully interpreted with this model.

1. Introduction

In passive microwave remote sensing of earth terrain, the random medium model has been developed to account for the volume scattering effects that are found to be extremely important. Both the wave theory [1-3] and the radiative transfer theory [4-5] have been applied in the calculation of the scatttering coefficients for active remote sensing and the emissivitties for passive remote sensing.

For terrain media such as sea ice [6-7], vegetation fields with row structures [8], and vegetation canopy with preferred azimuthal directions [9], the random medium must be characterized with an anisotropic permittivity tensor. Lee and Kong [10] have considered anisotropy in both the background permittivities and the randomly fluctuating parts. The backscattering coefficients for active remote sensing were calculated and applied to the interpretation of radar measurements from Arctic sea ice.

In this paper, we will apply the principle of reciprocity to calculate the emissivities [11] for passive microwave remote sensing. Making use of the dyadic Green's function for a two-layer anisotropic medium [12] and the first order Born approximation, we first obtain analytical expressions for the bistatic scattering coefficients. We then integrate over the upper hemisphere and subtract from unity to obtain the emissivities.

The angular responses of the emissivities are illustrated numerically by studying their dependence on the variance, the correlation lengths, and the mean permittivities, all of which can be anisotropic. The theoretical results are then used to interpret experimental data collected from vegetation fields where cut corn stalks are laid on the ground to emphasize their azimuthal dependence. The measured radiometric brightness temperatures will be shown to match with the theoretical results along different azimuthal angles of observation.

2. Formulation of the Problem

Consider an electromagnetic plane wave with a linearly polarized time-harmonic field

$$\bar{E}_{0i}(\bar{r},t) = \bar{E}_{0i}e^{i(\bar{k}_{oi}\cdot\bar{r}-\omega t)} \tag{2.1}$$

incident upon a layer of an anisotropic random medium with a permittivity tensor

$$\bar{\bar{\epsilon}}_1(\bar{r}) = <\bar{\bar{\epsilon}}_1(\bar{r})> + \bar{\bar{\epsilon}}_{1f}(\bar{r}) \tag{2.2}$$

where $<\bar{\bar{\epsilon}}_1(\bar{r})>$ is the mean part and $\bar{\bar{\epsilon}}_{1f}(\bar{r})$ represents the randomly fluctuating part [Fig. 1]. For the statistically homogeneous medium, $<\bar{\bar{\epsilon}}_1(\bar{r})>$ will be a constant independent of position, and $\bar{\bar{\epsilon}}_{1f}(\bar{r})$ is a random function of position whose ensemble average, $<\bar{\bar{\epsilon}}_{1f}(\bar{r})> = 0$. It is assumed that the amplitude of $\bar{\bar{\epsilon}}_{1f}(\bar{r})$ is small compared with $<\bar{\bar{\epsilon}}_1(\bar{r})>$. In general, both $<\bar{\bar{\epsilon}}_1(\bar{r})>$ and $\bar{\bar{\epsilon}}_{1f}(\bar{r})$ are taken to be uniaxial with the optic axis tilted off the z-axis by angles ψ and ψ_f, respectively, as shown in Fig. 2. The expressions for $<\bar{\bar{\epsilon}}_1(\bar{r})>$ and $<\bar{\bar{\epsilon}}_{1f}(\bar{r})>$ are given in Ref. [10].

The layer of random medium has boundaries at $z = 0$ and $z = -d$. The upper region is free space with permittivity ϵ_0. The lower region is homogeneous and isotropic with permittivity ϵ_2. All three regions are assumed to have the same permeability μ.

Expressing the electric fields in all regions in terms of the dyadic Green's functions and applying the first-order Born approximation as explained in detail in [10], the first-order scattered electric field intensity in region 0 is given by

$$<\left|\bar{E}_0^s(\bar{r})\right|^2> \approx <\left|\bar{E}_0^{(1)}(\bar{r})\right|^2> = \iint_V d^3\bar{r}_1\, d^3\bar{r}_2 \left\langle \left[\bar{\bar{G}}_{01}(\bar{r},\bar{r}_1)\cdot\bar{\bar{Q}}(\bar{r}_1)\cdot\bar{E}_1^{(0)}(\bar{r}_1)\right]\cdot\left[\bar{\bar{G}}_{01}(\bar{r},\bar{r}_2)\cdot\bar{\bar{Q}}(\bar{r}_2)\cdot\bar{E}_1^{(0)}(\bar{r}_2)\right]\right\rangle \tag{2.3}$$

where $\bar{\bar{G}}_{01}(\bar{r},\bar{r}_1)$ is the dyadic Green's function with the observation point in region 0 and the source point in region 1, $\bar{\bar{Q}}(\bar{r}) = \omega^2\mu\bar{\bar{\epsilon}}_{1f}(\bar{r})$ is the fluctuation tensor which stands for an effective source distribution, and $\bar{E}_1^{(0)}(\bar{r})$ is the unperturbed electric field in region 1 in the absence of fluctuation. $\bar{\bar{G}}_{01}(\bar{r},\bar{r}_1)$ and $\bar{E}_1^{(0)}(\bar{r})$ are obtained in Section 3 of [10] and the correlation functions of the tensor $\bar{\bar{Q}}$ are explained in Section 4 of [10].

3. Bistatic Scattering Coefficients and Emissivity

After the $\bar{\rho}_1$ -, $\bar{\rho}_2$ -, and $\bar{\beta}_\perp$ - integrations are performed as shown in [10], (2.3) reduces to

$$< \left|\bar{E}_0^s(\bar{r})\right|^2 >= \frac{A\left|\bar{E}_{0i}\right|^2 k_1'^4}{4r^2}\sum_{\substack{i,j,k\\l,m}}\int_{-\infty}^{\infty}d\bar{\beta}_z\iint_{-d}^{0}dz_1dz_2$$
$$g_{ij}(z_1)F_k(z_1)g_{il}^*(z_2)F_m^*(z_2)\Phi_{jklm}(\bar{\beta}_- = \bar{k}_{\rho i} - \bar{k}_\rho, \beta_z)e^{-i\beta_z(z_1-z_2)} \quad (3.1)$$

where Φ is the spectral density of the correlation function and all the constants and functions are defined in [10]. Now we have to evaluate the integral of the following form:

$$I = \int_{-\infty}^{\infty}d\beta_z\int_{-d}^{0}dz_1\int_{-d}^{0}dz_2 e^{i(-k_{1z}^p+k_{1z_1}^q-\beta_z)z_1}e^{-i(-k_{1z}^{r*}-k_{1z_1}^{t*}-\beta_z)z_2}\Phi(\beta_z)e^{-i\beta_z(z_1-z_2)} \quad (3.2)$$

$$= \int_{-\infty}^{\infty}d\beta_z\Phi(\beta_z)\frac{\left[1-e^{-id(-k_{1z}^p+k_{1z_1}^q-\beta_z)}\right]\left[1-e^{-id(k_{1z}^{r*}+k_{1z_1}^{t*}-\beta_z)}\right]}{(-k_{1z}^p+k_{1z_1}^q-\beta_z)(-k_{1z}^{r*}+k_{1z_1}^{t*}-\beta_z)} \quad (3.3)$$

where

$$\left\{\begin{matrix}p\\s\end{matrix}\right\} = \begin{cases}ou; & k_{1z}=k_{1z}^o\\ od; & k_{1z}=-k_{1z}^o\\ eu; & k_{1z}=k_{1z}^{eu}\\ ed; & k_{1z}=k_{1z}^{ed}\end{cases} \quad (3.4a)$$

$$\begin{Bmatrix} q \\ t \end{Bmatrix} = \begin{cases} ou; & k_{1zi} = k^{o}_{1zi} \\ od; & k_{1zi} = -k^{o}_{1zi} \\ eu; & k_{1zi} = k^{eu}_{1zi} \\ ed; & k_{1zi} = k^{ed}_{1zi} \end{cases} \tag{3.4b}$$

The β_z-integration will be performed term by term using the contour integration of residue calculus. We pick up the dominant pole contributions under some approximations reasonable in the microwave remote sensing of earth terrain, as described in the paper [10]. The value of integration is significant only when $p = s$ and $q = t$, or when $p = t^{+}$ and $q = s^{+}$ for the backscattered direction. The final result is the following:

$$I \approx \begin{cases} 2\pi\Phi(\beta_z = -k'^{p}_{1z} - k'^{q}_{1zi}) \dfrac{e^{2(-k''^{p}_{1z} + k''^{q}_{1zi})d} - 1}{2(-k''^{p}_{1z} + k''^{q}_{1zi})} & \text{for } p = s,\ q = t \qquad (3.5a) \\ 2\pi\Phi(\beta_z = k'^{t}_{1zi} + k'^{q}_{1zi}) \dfrac{e^{2(k''^{t}_{1zi} + k''^{q}_{1zi})d} - 1}{2(k''^{t}_{1zi} - k''^{q}_{1zi})} & \text{for } p = t^{+},\ q = s^{+} \text{and backscattering} \qquad (3.5b) \\ 2\pi\Phi(\beta_z = 0)d, & \text{only when } k^{p}_{1z} = k^{q}_{1zi} \text{ and } k^{s}_{1z} = k^{t}_{1zi} \qquad (3.5c) \end{cases}$$

where the operator $^{+}$ transforms $od \leftrightarrow ou$ and $ed \leftrightarrow eu$, and where $'$ denotes the real part and $''$ denotes the imaginary part of that quantity.

Making use of (3.5) for evaluation of the integral in (3.3), we obtain the bistatic scattering coefficients, which are defined by Peake [11] as

$$\gamma_{\beta\alpha}(\bar{k}_s, \bar{k}_{oi}) \equiv \lim_{\substack{A\to\infty \\ r\to\infty}} \frac{4\pi r^2 < \left|\bar{E}^{s}_{0}(\bar{r})\right|^2 >_{\alpha}}{A\cos\theta_{oi}\ \left|\bar{E}_{0i}\right|^2_{\beta}}, \qquad \alpha, \beta = \begin{Bmatrix} H \\ V \end{Bmatrix} \tag{3.6}$$

where $\left|\bar{E}_{oi}\right|^2_{\beta}$ is the incident electric field intensity with polarization β, $< \left|\bar{E}^{s}_{0}(\bar{r})\right|^2 >_{\alpha}$ is the mean scattered field intensity with polarization α, $\bar{k}_{oi}$ is the incident wave vector at incidence angles (θ_{oi}, ϕ_{oi}) and $\bar{k}_s$ is the scattered wave vector at scattered angles (θ_s, ϕ_s). The final results are as follows:

$$\gamma_{\beta\alpha} = \frac{2\pi^2 k'^{4}_{1}}{\cos\theta_{oi}} \sum_{i=1}^{11} J_i \tag{3.7}$$

where the expressions for J_i's are given in the Appendix.

By using energy conservation and reciprocity arguments, we can express the emissivity at angle (θ_{oi}, ϕ_{oi}) with β-polarization in the following form [11]:

$$e_\beta(\theta_{oi}, \phi_{oi}) = 1 - A_\beta(\theta_{oi}, \phi_{oi}), \qquad \beta = H \text{ or } V \tag{3.8a}$$

$$= 1 - r_{\beta c}(\theta_{oi}, \phi_{oi}) - r_{\beta i}(\theta_{oi}, \phi_{oi}) \tag{3.8b}$$

where $A_\beta(\theta_{oi}, \phi_{oi})$ is an "albedo" defined as the fraction of the power incident on the surface from the direction (θ_{oi}, ϕ_{oi}) at β-polarization that is reflected or rescattered, $r_{\beta c}(\theta_{oi}, \phi_{oi})$ is the "coherent reflectivity" which denotes the fraction of the power reflected in a specular direction, and $r_{\beta i}(\theta_{oi}, \phi_{oi})$ is the "incoherent reflectivity" which denotes the fraction of the power scattered over the upper hemisphere. The reflectivities are given by

$$r_{\beta c}(\theta_{oi}, \phi_{oi}) = \sum_{\alpha = H,V} |R_{\beta\alpha i}(\theta_{oi}, \phi_{oi})|^2 \tag{3.9a}$$

$$r_{\beta i}(\theta_{oi}, \phi_{oi}) = \frac{1}{4\pi} \sum_{\alpha = H,V} \int_0^{2\pi} d\phi \int_0^{\frac{\pi}{2}} d\theta \sin\theta \gamma_{\beta\alpha}(\theta_{oi}, \phi_{oi}; \theta, \phi) \tag{3.9b}$$

where $\gamma_{\beta\alpha}$ is given in (3.7) and $R_{\beta\alpha i}$ is calculated in Ref [12] as follows:

$$R_{\beta\alpha i} = R_{01\beta\alpha} - X_{\beta o}(L_1 o_o - M_2 e_o) X_{o\alpha} - X_{\beta o}(L_1 o_e - M_2 e_e) X_{e\alpha}$$
$$- X_{\beta e}(L_2 o_o + M_1 e_o) X_{o\alpha} - X_{\beta e}(L_2 o_e + M_1 e_e) X_{e\alpha} \tag{3.10}$$

where all the coefficients are defined in [12] and should be evaluated at angles of incidence (θ_{oi}, ϕ_{oi}).

4. Discussion and Application of the Results

First, it can be easily shown that (3.7) reduces to (5.24)-(5.32) of the paper [10] when $\theta_s = \theta_{oi}$ and $\phi_s = \pi - \phi_{oi}$, which are the results for the backscattering coefficients. Also, in the limiting

case when both the mean and fluctuation are isotropic, i.e. when $\epsilon_{1z} = \epsilon_1$, $\epsilon_{1zf} = \epsilon_{1f}$, and $\psi = \psi_f = 0$, the result (3.7) reduces to

$$\gamma_{HH} = \frac{\pi^2 k_1'^4}{\cos\theta_{oi}} \left| \frac{X_{10} X_{01i}}{D_2 D_{2i}} \right|^2 \left| \frac{k_{oz}}{k_{1z}} \right|^2 \cos^2(\phi_s - \phi_{oi})$$
$$\left\{ \frac{1 - e^{-2(k_{1z}'' + k_{1zi}'')d}}{k_{1z}'' + k_{1zi}''} \Phi(\bar{\beta}_+) \left[1 + |R_{12} R_{12i}|^2 e^{-2(k_{1z}'' + k_{1zi}'')d} \right] \right.$$
$$\left. + \frac{1 - e^{-2(k_{1zi}'' - k_{1z}'')d}}{k_{1zi}'' - k_{1z}''} \Phi(\bar{\beta}_-) \left[|R_{12i}|^2 e^{-2(k_{1zi}'' - k_{1z}'')d} + |R_{12}|^2 e^{-4k_{1z}'' d} \right] \right\}$$
$$+ \Delta \frac{4\pi^2 k_1'^4}{\cos\theta_{oi}} \left| \frac{X_{01i}}{D_{2i}} \right|^4 |R_{12i}|^2 e^{-4k_{1zi}'' d} \Phi(\bar{\beta}_o) d \qquad (4.1a)$$

$$\gamma_{VV} = \frac{\pi^2 k_1'^4}{\cos^2\theta_{oi}} \left| \frac{Y_{10}}{F_2} \frac{Y_{01i}}{F_{2i}} \right|^2 \left| \frac{k_{oz}}{k_{1z}} \right|^2 \left| \frac{k_o}{k_1} \right|^4$$
$$\left\{ \frac{1 - e^{-2(k_{1z}'' + k_{1zi}'')d}}{k_{1z}'' + k_{1zi}''} \Phi(\bar{\beta}_+) \left[1 + |S_{12} S_{12i}|^2 e^{-2(k_{1z}'' + k_{1zi}'')d} \right] \right.$$
$$\left. \cdot \left| \frac{k_{1z} k_{1zi}}{k_o^2} \cos(\phi_s - \phi_{oi}) - \sin\theta_s \sin\theta_{oi} \right|^2 \right.$$
$$\left. + \frac{1 - e^{-2(k_{1zi}'' - k_{1z}'')d}}{k_{1zi}'' - k_{1z}''} \Phi(\bar{\beta}_-) \left[|S_{12i}|^2 e^{-2(k_{1z}'' - k_{1zi}'')d} + |S_{12}|^2 e^{-4k_{1z}'' d} \right] \right.$$
$$\left. \cdot \left| \frac{k_{1z} k_{1zi}}{k_o^2} \cos(\phi_s - \phi_{oi}) + \sin\theta_s \sin\theta_{oi} \right|^2 \right\}$$
$$+ \Delta \frac{4\pi^2 k_1'^4}{\cos\theta_{oi}} \left| \frac{Y_{01i}}{F_{2i}} \right|^4 \left| \frac{k_o}{k_1} \right|^8 |S_{12i}|^2 e^{-4k_{1zi}'' d} \Phi(\bar{\beta}_o) d \left| \frac{k_{1zi}^2}{k_o^2} - \sin^2\theta_{oi} \right|^2 \qquad (4.1b)$$

$$\gamma_{HV} = \frac{\pi^2 k_1'^4}{\cos\theta_{oi}} \left| \frac{Y_{10} X_{01i}}{F_2 D_{2i}} \right|^2 \left| \frac{k_{oz}}{k_o} \right|^2 \sin^2(\phi_s - \phi_{oi})$$
$$\left\{ \frac{1 - e^{-2(k_{1z}'' + k_{1zi}'')d}}{k_{1z}'' + k_{1zi}''} \Phi(\bar{\beta}_+) \left[1 + |S_{12} R_{12i}|^2 e^{-2(k_{1z}'' + k_{1zi}'')d} \right] \right.$$
$$\left. + \frac{1 - e^{-2(k_{1zi}'' - k_{1z}'')d}}{k_{1zi}'' - k_{1z}''} \Phi(\bar{\beta}_-) \left[|R_{12i}|^2 e^{-2(k_{1zi}'' + k_{1z}'')d} + |S_{12}|^2 e^{-4k_{1z}'' d} \right] \right\} \qquad (4.1c)$$

$$\gamma_{VH} = \frac{\pi^2 k_1'^4}{\cos\theta_{oi}} \left| \frac{X_{10} Y_{01i}}{D_2 F_{2i}} \right|^2 \left| \frac{k_{oz} k_o k_{1zi}}{k_{1z} k_1^2} \right|^2 \sin^2(\phi_s - \phi_{oi})$$
$$\left\{ \frac{1 - e^{-2(k_{1z}'' + k_{1zi}'')d}}{k_{1z}'' + k_{1zi}''} \Phi(\bar{\beta}_+) \left[1 + |R_{12} S_{12i}|^2 e^{-2(k_{1z}'' + k_{1zi}'')d} \right] \right.$$
$$\left. + \frac{1 - e^{-2(k_{1zi}'' - k_{1z}'')d}}{k_{1zi}'' - k_{1z}''} \Phi(\bar{\beta}_-) \left[|S_{12i}|^2 e^{-2(k_{1zi}'' + k_{1z}'')d} + |R_{12}|^2 e^{-4k_{1z}'' d} \right] \right\} \qquad (4.1d)$$

where

$$\bar{\beta}_+ = (\bar{k}_{\rho i} - \bar{k}_\rho) + \hat{z}(k_{1zi}' - k_{1z}')$$

$$\bar{\beta}_- = (\bar{k}_{\rho i} - \bar{k}_\rho) + \hat{z}(k_{1zi}' - k_{1z}')$$

$$\bar{\beta}_o = 2\bar{k}_{\rho i}$$

and Δ is defined in the appendix.

These results are exactly the same as those for bistatic scattering coefficients obtained in the case of two-layer isotropic random media by Zuniga and Kong [13]. It is interesting to note that our results can be shown, with some algebraic manipulation, to satisfy the following four relations:

$$\cos\theta_{oi} \gamma_{\beta\alpha}(i,s) = \cos\theta_s \gamma_{\alpha\beta}(s,i), \qquad \beta, \alpha = H \text{ or } V \qquad (4.2)$$

where the first lettter in the brackets indicates the direction from which the radiation is incident, and the second letter indicates the direction into which the radiation is scattered. This is a consequence of the reciprocity theorem [11] as the anisotropic random medium is reciprocal and its permittivity tensor is symmetric.

As an illustration of our theoretical results, the emissivities e_H and e_V are plotted as a function of the incidence angle at 10 GHz in Fig. 3-4. The correlation function is assumed to be exponential in both the lateral and the vertical directions and it is assumed that $\psi = \psi_f$ as in [10]. The dependence of the emissivity on the azimuthal incidence angle ϕ_{oi} as shown in Fig. 3 is

a clear indication of the medium anisotropy. When $\delta_1 > \delta_2$, the strength of fluctuation is stronger in the lateral direction (the plane perpendicular to the optic axis) than in the vertical direction (along the optic axis of fluctuation). Then for large azimuthal incidence angles ($\phi_{oi} = 80^\circ$), the H -polarized wave, whose electric field is almost directed laterally, is scattered more, resulting in smaller emissivity. On the other hand, the V -polarized wave is scattered less for large ϕ_{oi}, resulting in higher emissivity.

In Fig. 4, for large $\phi_{oi}(= 80^\circ)$, when ϵ''_{1z} is increased from 0.02 to 0.1, e_H remains approximately the same, but e_V increases noticably. It is due to the anisotropy of mean permittivity. When the loss in the vertical direction is increased, the H -polarization is not significantly affected, but the V -polarization, which has components in the vertical direction, will experience more of the absorption effect, resulting in higher emission.

As an application of our theoretical results, we choose to interpret the field data of series 3 obtained by NASA and USDA at BARC (Betsville Agricultural Research Center) with their 1982 corn destruction experiments [14-15]. The corn stalks above the ground were cut and removed, and the brightness temperature is measured with a radiometer for the stubble ground. Then the stalks were laid down on the ground and aligned in specific orientations. The measurements were made with the radiometer looking parallel and perpendicular to the row direction of corn stalks at two frequency bands, the L-band (1.4 GHz) and the C-band (5 GHz). Because the corn stalks have a preferred orientation in the horizontal plane, they are modelled as an anisotropic random layer with the optic axis in the horizontal plane ($\psi = \psi_f = 90^\circ$). As is clearly seen in Figs. 5-10, the theory explains fairly well the data behavior at different angles of incidence, polarizations, frequencies, and orientations. The letters V and H denote the experimental data and the curves denote the theoretical results. All six sets of data are matched with a single set of parameters: $\delta_1 = 0.03$, $\delta_2 = 0.075$, $l_\rho = 2\,\text{cm}$, $l_z = 15\,\text{cm}$, and with the permittivities of the stalk layer and the ground following the frequency-dependence, as given by Ulaby and Jedlicka [16].

In the calculation of the brightness temperature, the following relation is used, assuming uniform temperature distribution T_o :

$$T_B^{(\beta)} = e_\beta T_o \tag{4.3}$$

where β is the state of polarization to be considered and T_o is the physical temperature of the ground in $^\circ K$.

We first observe, by comparing Fig. 6 and Fig. 9 (stalks-covered) with Fig. 5 and Fig. 8 (stubble), respectively, that the brightness temperatures have greatly increased, on account of the corn stalk layer. Second, by comparing Fig. 7 ($\phi_{oi} = 0°$) with Fig. 6 ($\phi_{oi} = 90°$) at 1.4GHz, we see that the horizontal polarization increases and the vertical polarization decreases, both so substantially that there is a crossover between curves of $T_B^{(H)}$ and $T_B^{(V)}$. This phenomenon can be explained by the anisotropy of the dielectric loss of the corn layer where $\epsilon_{1z}'' > \epsilon_1''$. For an azimuthal observation angle perpendicular to the stalk orientation ($\phi_{oi} = 0^\circ$), the horizontal polarization has an $\overline{E}$ field parallel to the stalk and the vertical polarization has $\overline{E}$ perpencicular to the stalk. Then the H-polarization experiences more absorptions than the V-polarization, resulting in an increase of the brightness termperature for the H-polarization and a decrease for the V-polarization.

Third, we compare Fig. 10 ($\phi_{oi} = 90^\circ$) with Fig. 9 ($\phi_{oi} = 0^\circ$) at 5GHz. It is seen that the horizontal polarization increases, wheras the vertical polarization decreases. The responses are completely opposite from those in the case of the L-band ($f = 1.4$GHz). For the C-band, where the dielectric loss is chosen to be smaller, the scattering effect is dominant over the absorption effect for both polarizations. With this in mind, the opposite responses can be explained by the anisotropic fluctuation of the stalk layer where $\delta_1 < \delta_2$. For observation angles parallel to the stalk orientation ($\phi_{oi} = 90^\circ$), the horizontal polarization has an $\overline{E}$ field perpendicular to the stalk.

whereas the vertical polarization has $\overline{E}$-components parallel to the stalk. Due to the stronger fluctuation along the stalk (δ_2), the H-polarization experiences less scattering whereas the V-polarization experiences more; hence, the result is an increase in T_B for the H-polarization and a decrease for the V-polarization.

5. Conclusions

With the use of the dyadic Green's functions, a two-layer anisotropic random medium has been studied and applied to the passive remote sensing of earth terrain media. Applying the first-order Born approximation, the bistatic scattering coefficients are obtained in analytical forms. The emissivities are then computed by invoking the principle of reciprocity. It is shown that both the absorptive and randomly fluctuating properties of the anisotropic medium affect the behavior of the resulting brightness temperatures both in theory and in actual controlled field measurements. The theoretical results are favorably matched with the experimental data obtained from the corn stalks with detailed ground truth information. When and if such ground truth is available for sea ice measurements, the theoretical model is ideal for the interpretation of the experimental data as sea ice is also a highly anisotropic random medium.

REFERENCES

[1] A. Stogryn, " Electromagnetic scattering by random dielectric constant fluctuations in a bounded medium," *Radio Science*, **9**, 509–518, May 1974 .

[2] L. Tsang and J. A. Kong , " Emissivity of half-space random media," *Radio Science*, **11**, 593–598, July 1976 .

[3] A. K. Fung and H. S. Fung , " Application of first-order renormalization method to scattering from a vegetated-like half-space," *IEEE Trans. Geosci. Electron.*, **GE–15**, 189–195, Oct. 1977 .

[4] L. Tsang and J. A. Kong , " Thermal microwave emission from half-space random media," *Radio Science*, **11**, 599–609, July 1976 .

[5] S. L. Chuang, J. A. Kong, and L. Tsang , " Radiative transfer theory for passive microwave remote sensing of a two-layer random medium with cylindrical structures," *J. Appl. Phys.*, **51**, 5588–5593, Nov. 1980 .

[6] W. M. Sackinger and R. C. Byrd, "Reflection of millimeter waves from snow and sea ice," *IAEE Report* **7203**, Institute of Arctic Environmental Engineering, Univ. of Alaska, Jan. 1972 .

[7] R. G. Onstott, R. K. Moore and W. F. Weeks, "Surface–based scatterometer results of Arctic sea ice," *IEEE Trans. Geosci. Electron.*, **GE–17**, 78–85, July 1979 .

[8] P. P. Batlivala and F. T. Ulaby , " Radar look direction and row crops," *Photogrammetric Eng. and Remote Sensing*, **42**, 233–238, Feb. 1976 .

[9] R. S. Loomis and W. A. Williams, "Productivity and the morphology of crop stands : Pattern with leaves," *Physiological Basis of Crop Yield*, edited by J. D. Eastin et al., American Society of Agronomy, Madison, WI, 1969 .

[10] J. K. Lee and J. A. Kong, "Active microwave remote sensing of an anisotropic random medium layer," *IEEE Trans. Geosci. Remote Sensing*, Submitted for publication .

[11] W. H. Peake, "Interaction of electromagnetic waves with some natural surfaces," *IRE Trans. Antennas Propagat.*, **AP 7**, S324-S329, Dec. 1959 .

[12] J. K. Lee and J. A. Kong, "Dyadic Green's functions for layered anisotropic medium," *Electromagnetics*, **3**, 111-130, April-June 1983 .

[13] M. A. Zuniga and J. A. Kong , " Active remote sensing of random media," *J. Appl. Phys.*, **51**, 74-79, Jan. 1980 .

[14] P. E. O'Neill, T. J. Jackson, B. J. Blanchard, J. R. Wang and W. I. Gould, "Effects of corn stalk orientation and water content on passive microwave sensing of soil moisture," *Remote Sensing of Environment*, **16**, 55-67, Aug. 1984 .

[15] P. O'Neill, T. Jackson, B. Blanchard, R. van den Hoek, W. Gould, J. Wang, W. Glazar and J. McMurtrey III, "The effects of vegetation and soil hydraulic properties on passive microwave sensing of soil moisture : Data report for the 1982 field experiments," *NASA Technical Memorandum* **85106**, National Aeronautics and Space Administration, Goddard Space Flight Center, Greenbelt, MD, Sept. 1983 .

[16] F. T. Ulaby and R. P. Jedlicka, " Microwave dielectric properties of plant materials," *IEEE Trans. Geosci. Remote Sensing*, **GE-22**, 406-415, July 1984 .

FIGURE CAPTIONS

Figure 1 Scattering geometry of a two-layer anisotropic random medium.

Figure 2 Geometrical configuration characterizing a permittivity tensor.

Figure 3 Incidence angle responses of emissivity due to the effect of anisotropic permittivity fluctuation when $\delta_1 > \delta_2$.

Figure 4 Incidence angle responses of emissivity due to the effect of anisotropic background permittivity when $\phi_{o1} = 80°$.

Figure 5 Interpretation of radiometric data for ground with stubbles at L band .

Figure 6 Interpretation of radiometric data for cut stalks parallel at L band .

Figure 7 Interpretation of radiometric data for cut stalks perpendicular at L band .

Figure 8 Interpretation of radiometric data for ground with stubbles at C band .

Figure 9 Interpretation of radiometric data for cut stalks perpendicular at C band .

Figure 10 Interpretation of radiometric data for cut stalks parallel at C band .

Figure 1

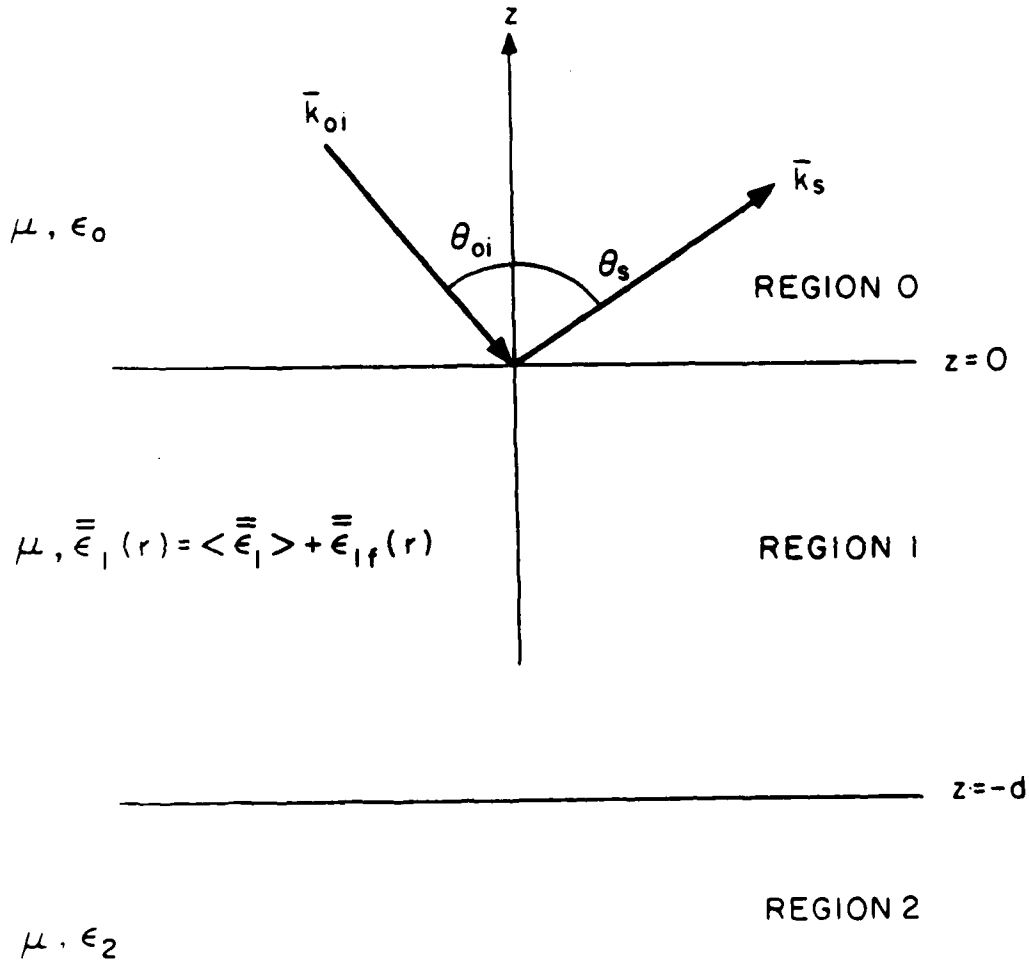
z
$\bar{k}_{oi}$
$\bar{k}_s$
θ_{oi}
θ_s
μ, ϵ_0
REGION 0
z = 0
$\mu, \bar{\bar{\epsilon}}_1(r) = <\bar{\bar{\epsilon}}_1> + \bar{\bar{\epsilon}}_{1f}(r)$
REGION 1
z = -d
REGION 2
μ, ϵ_2

Figure 2

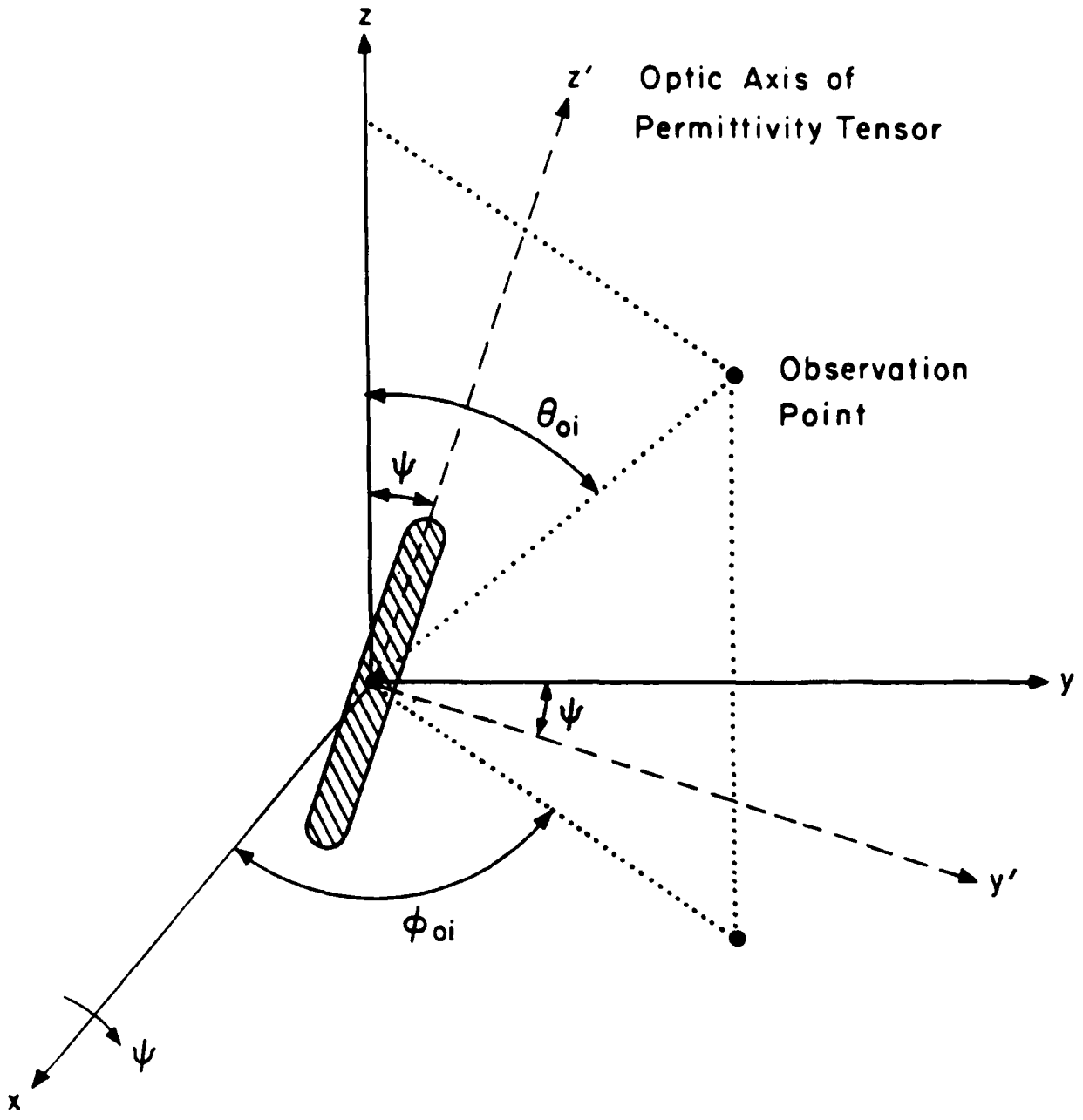
z
z'
Optic Axis of
Permittivity Tensor
Observation
Point
θ_{oi}
ψ
y
ψ
y'
ϕ_{oi}
ψ
x

Figure 3

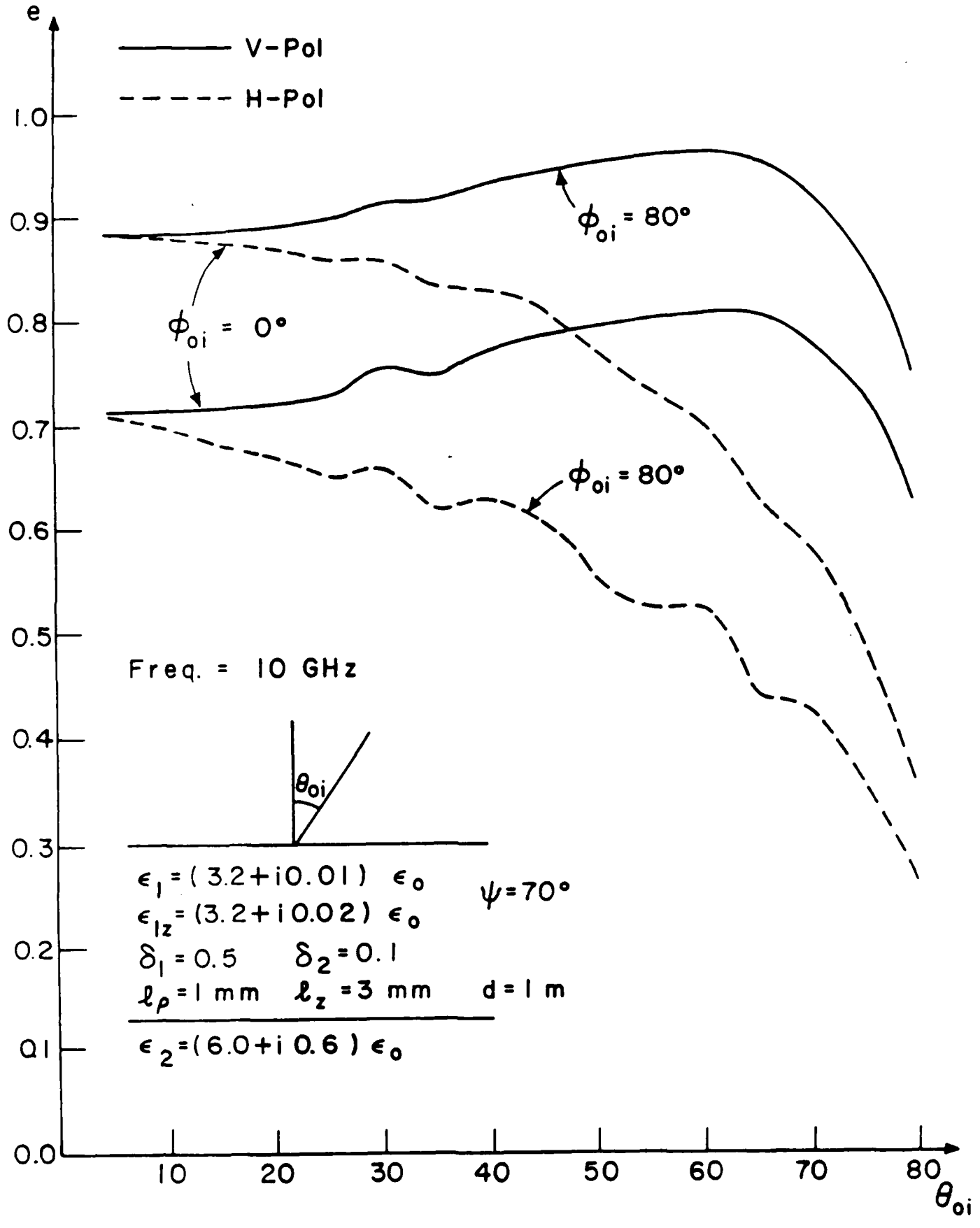
e
V-Pol
H-Pol
1.0
0.9
0.8
0.7
0.6
0.5
0.4
0.3
0.2
0.1
0.0
ϕ_{oi} = 80°
ϕ_{oi} = 0°
ϕ_{oi} = 80°
Freq. = 10 GHz
θ_{oi}
$\epsilon_1 = (3.2 + i0.01)\ \epsilon_0$
$\epsilon_{1z} = (3.2 + i0.02)\ \epsilon_0$
$\delta_1 = 0.5$ $\delta_2 = 0.1$
$\ell_\rho = 1$ mm $\ell_z = 3$ mm
$\epsilon_2 = (6.0 + i\,0.6)\ \epsilon_0$
$\psi = 70°$
d = 1 m
10
20
30
40
50
60
70
80
θ_{oi}

Figure 4

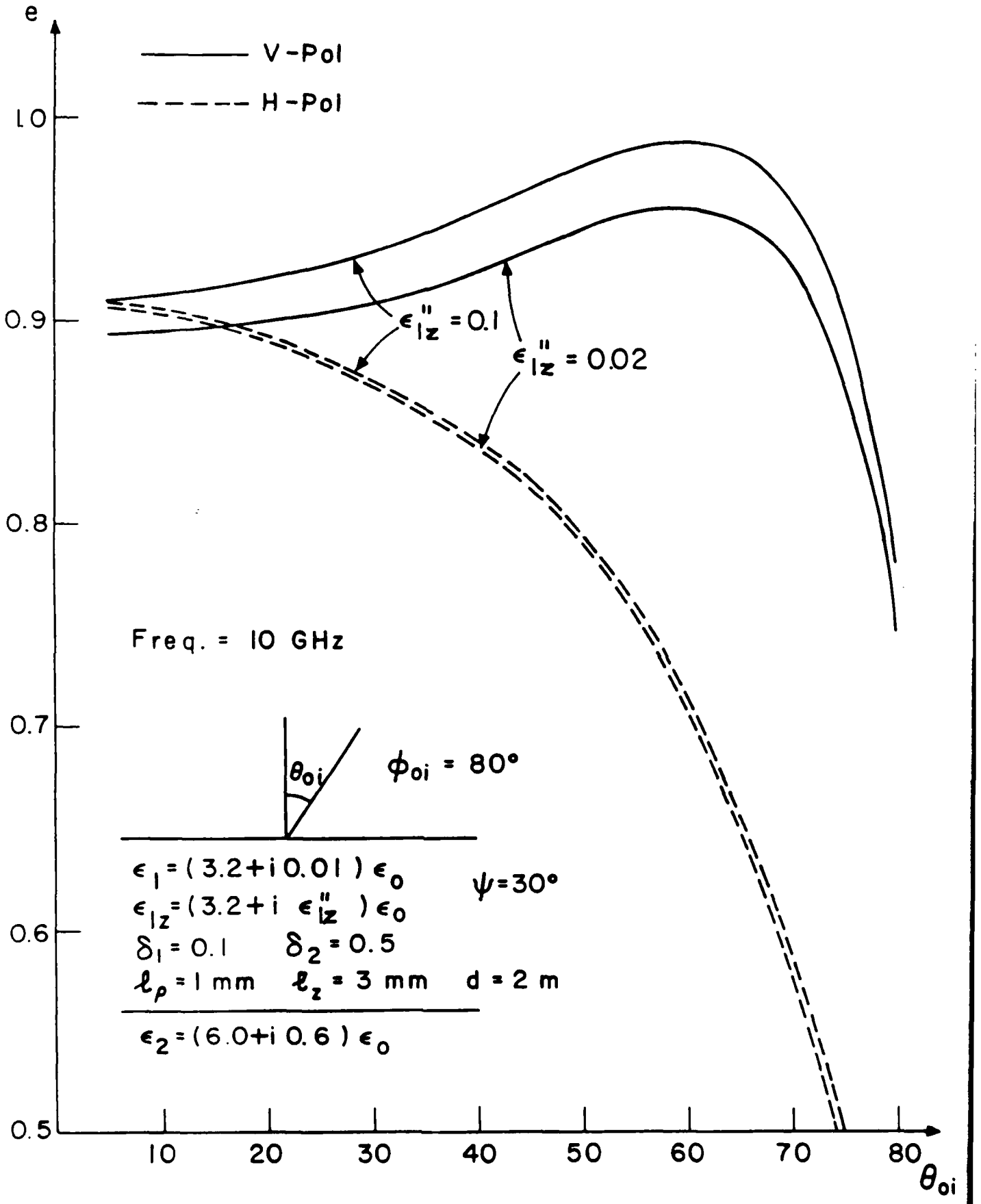
e
V-Pol
H-Pol
1.0
0.9
0.8
0.7
0.6
0.5
$\epsilon''_{1z} = 0.1$
$\epsilon''_{1z} = 0.02$
Freq. = 10 GHz
θ_{oi}
$\phi_{oi} = 80°$
$\epsilon_1 = (3.2 + i\,0.01)\,\epsilon_0$
$\psi = 30°$
$\epsilon_{1z} = (3.2 + i\,\epsilon''_{1z})\,\epsilon_0$
$\delta_1 = 0.1$ $\delta_2 = 0.5$
$\ell_\rho = 1$ mm $\ell_z = 3$ mm d = 2 m
$\epsilon_2 = (6.0 + i\,0.6)\,\epsilon_0$
10
20
30
40
50
60
70
80
θ_{oi}

Figure 5

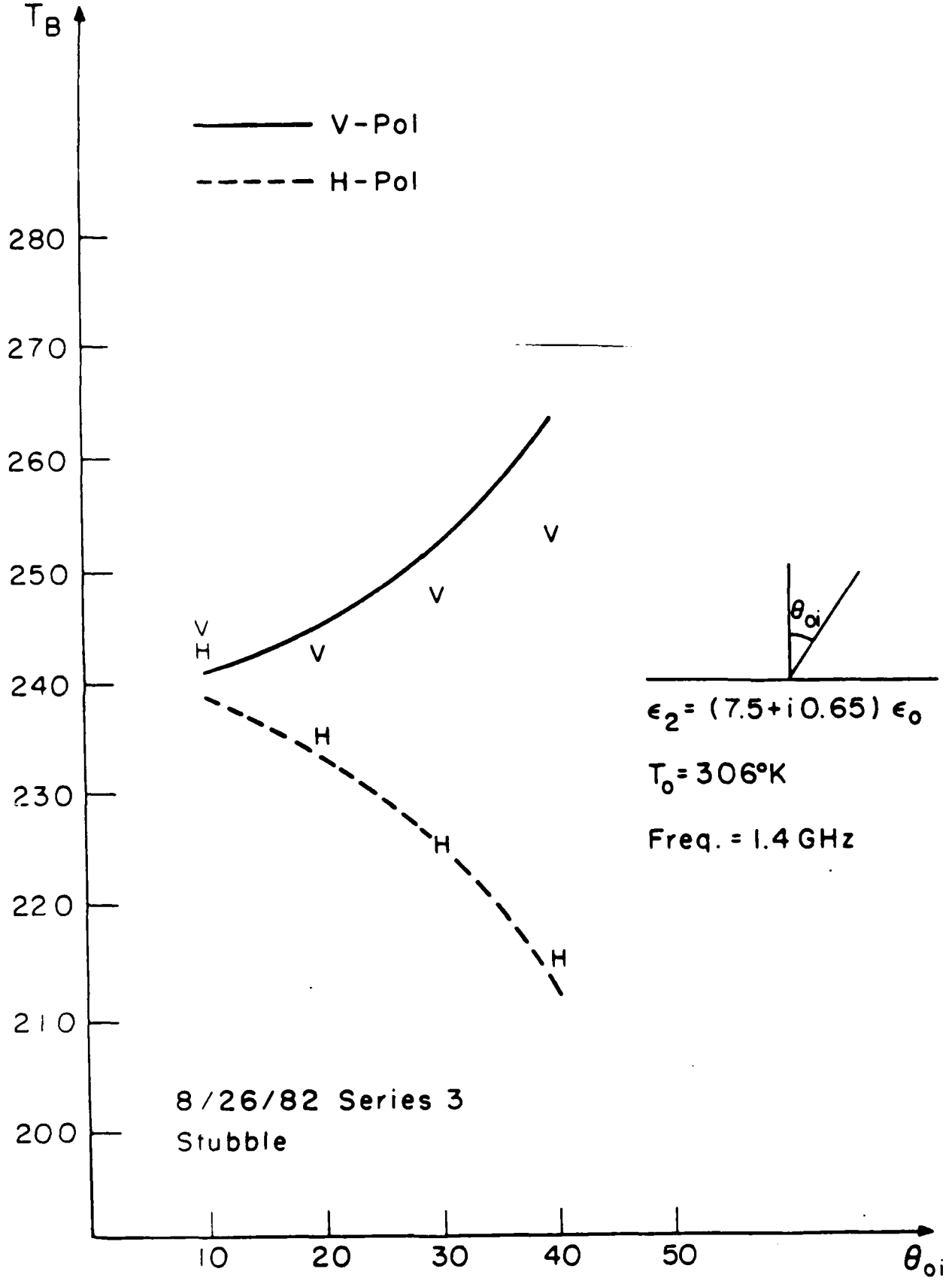
T_B
V-Pol
H-Pol
280
270
260
250
240
230
220
210
200
V
H
V
V
V
H
H
H
8/26/82 Series 3
Stubble
10
20
30
40
50
θ_{oi}
θ_{oi}
$\epsilon_2 = (7.5 + i\,0.65)\,\epsilon_o$
$T_o = 306°K$
Freq. = 1.4 GHz

Figure 6

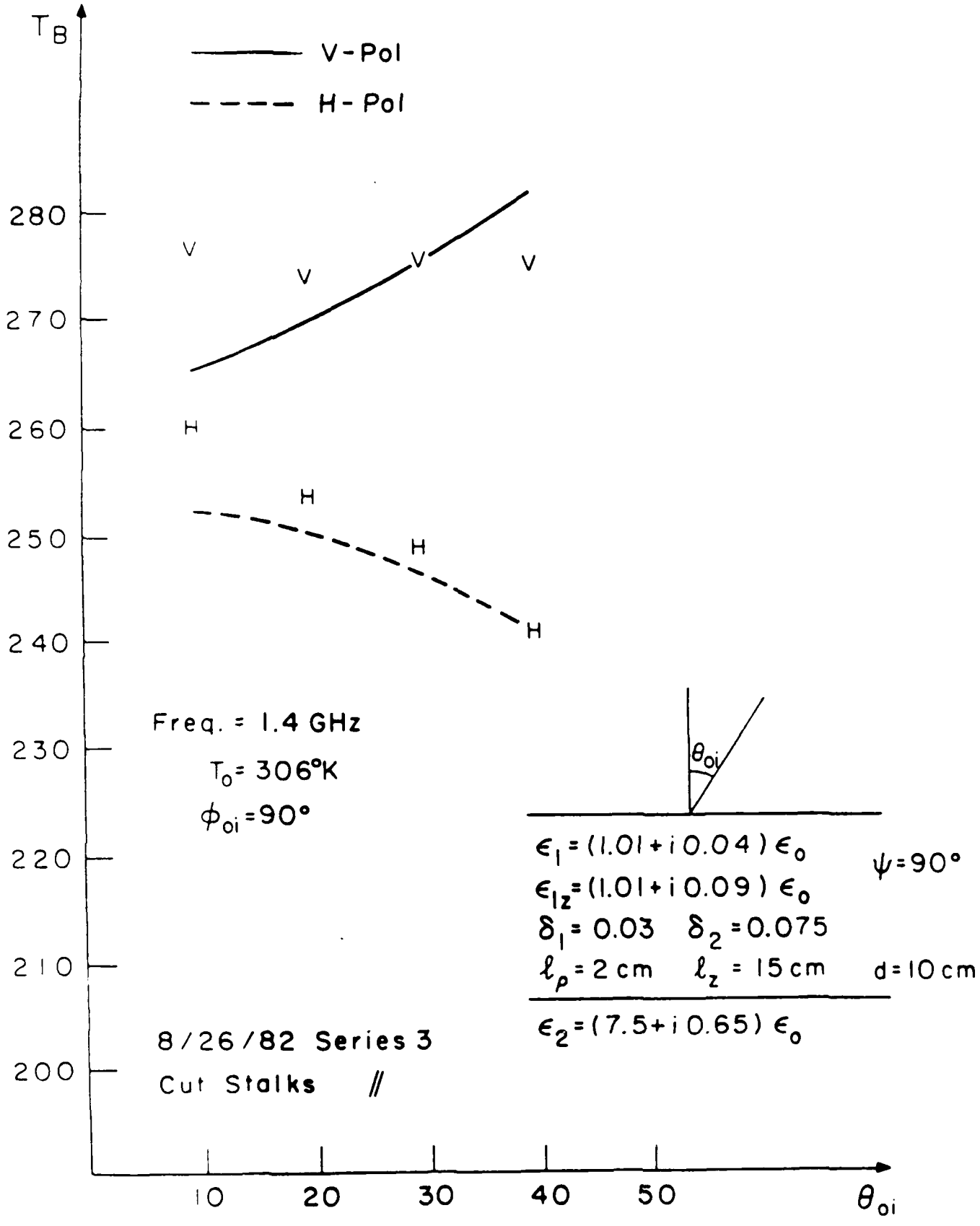
T_B
V-Pol
H-Pol
280
270
260
250
240
230
220
210
200
V
V
V
V
H
H
H
H
Freq. = 1.4 GHz
T_0 = 306°K
ϕ_{oi} = 90°
θ_{oi}
$\epsilon_1 = (1.01 + i\,0.04)\,\epsilon_0$
$\epsilon_{1z} = (1.01 + i\,0.09)\,\epsilon_0$
$\psi = 90°$
$\delta_1 = 0.03$ $\delta_2 = 0.075$
$\ell_\rho = 2$ cm $\ell_z = 15$ cm
d = 10 cm
$\epsilon_2 = (7.5 + i\,0.65)\,\epsilon_0$
8/26/82 Series 3
Cut Stalks //
10
20
30
40
50
θ_{oi}

Figure 7

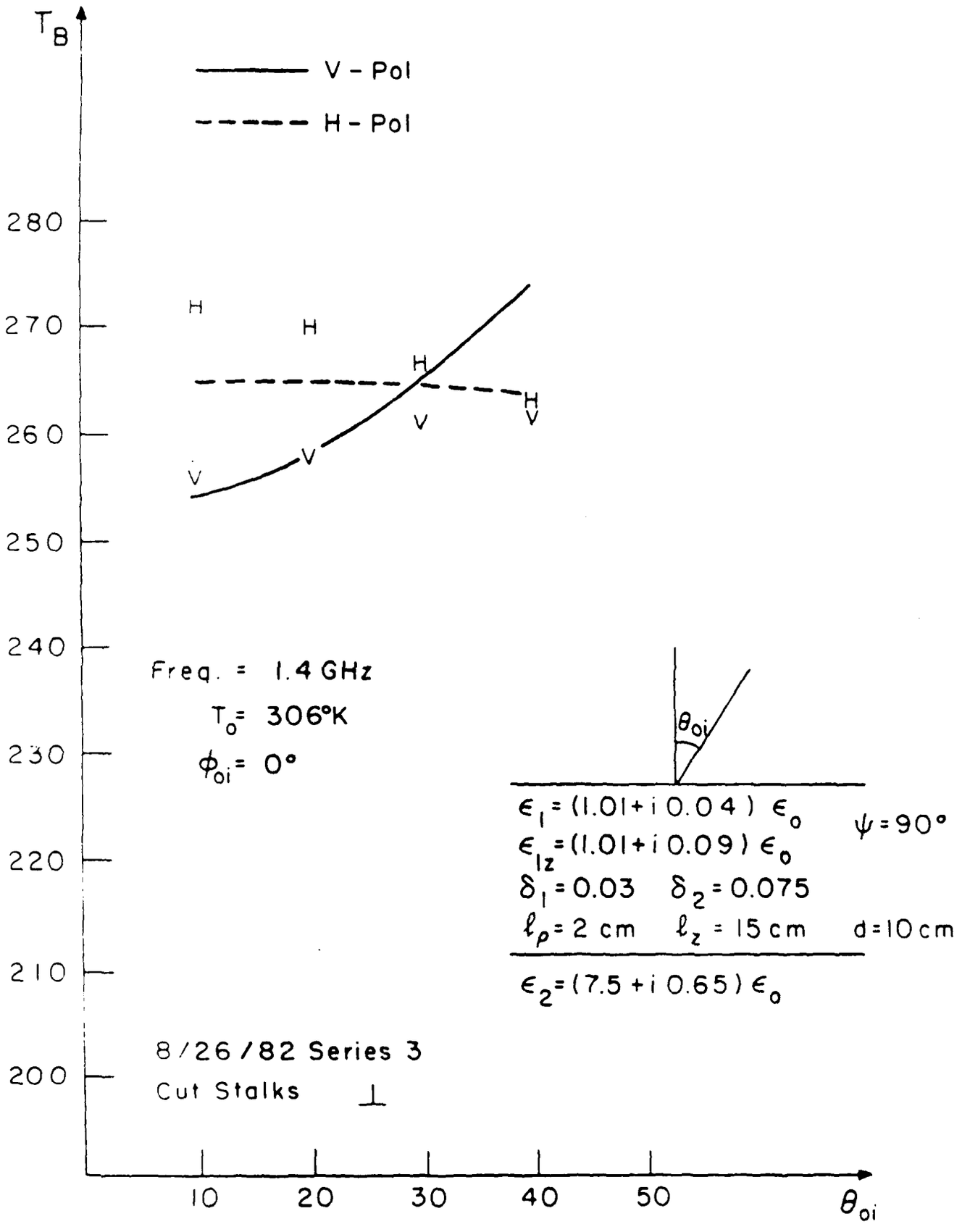
T_B
V - Pol
H - Pol
280
270
260
250
240
230
220
210
200
H
H
H
H
V
V
V
V
Freq. = 1.4 GHz
T_o = 306°K
ϕ_{oi} = 0°
θ_{oi}
$\epsilon_1 = (1.01 + i\,0.04)\,\epsilon_o$
$\epsilon_{1z} = (1.01 + i\,0.09)\,\epsilon_o$
$\psi = 90°$
$\delta_1 = 0.03$ $\delta_2 = 0.075$
$\ell_\rho = 2$ cm $\ell_z = 15$ cm
d = 10 cm
$\epsilon_2 = (7.5 + i\,0.65)\,\epsilon_o$
8/26/82 Series 3
Cut Stalks ⊥
10
20
30
40
50
θ_{oi}

Figure 8

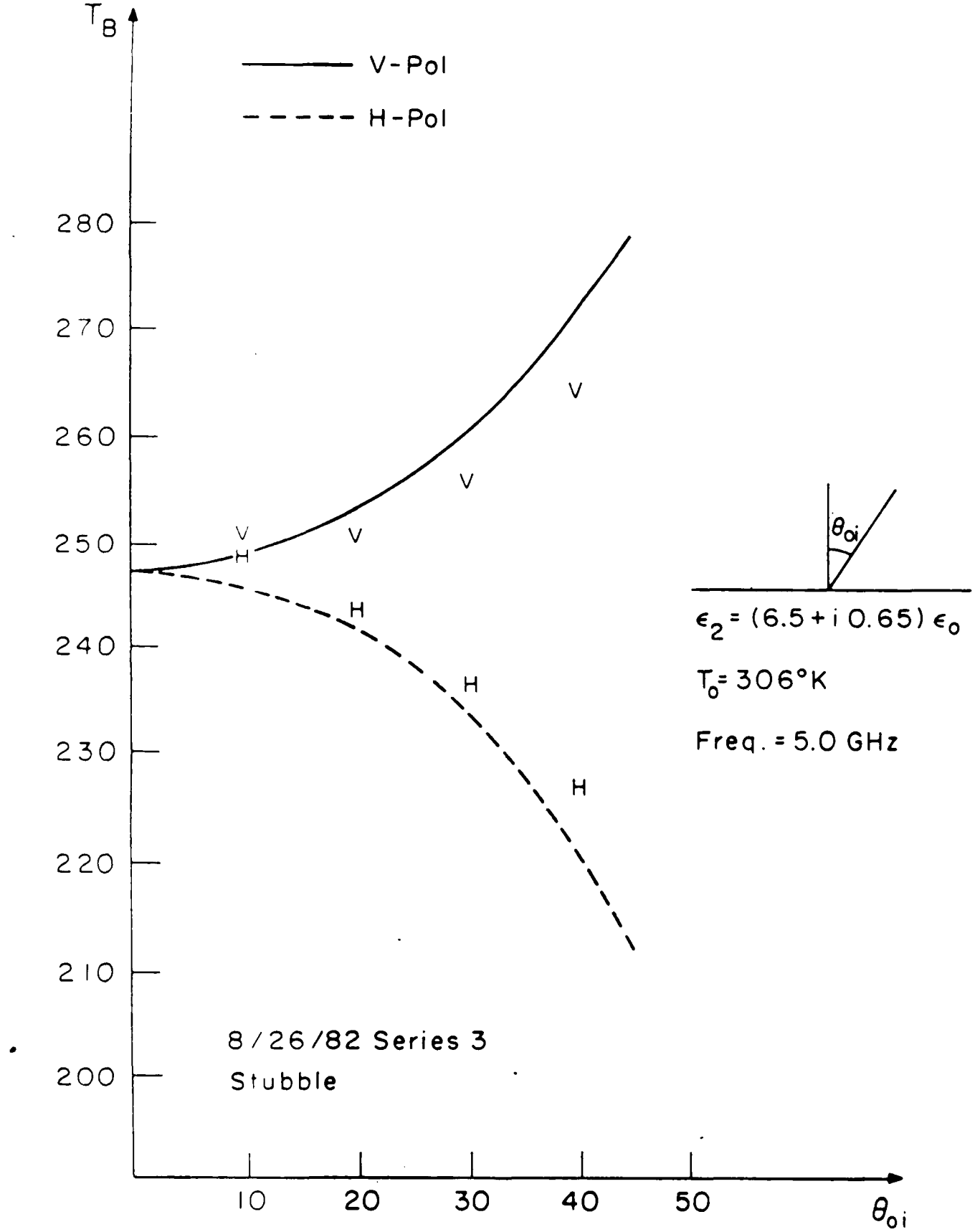
T_B
V-Pol
H-Pol
280
270
260
250
240
230
220
210
200
V
V
V
V
H
H
H
H
8/26/82 Series 3
Stubble
10
20
30
40
50
θ_{oi}
θ_{oi}
$\epsilon_2 = (6.5 + i\,0.65)\,\epsilon_o$
$T_o = 306°K$
Freq. = 5.0 GHz

Figure 9

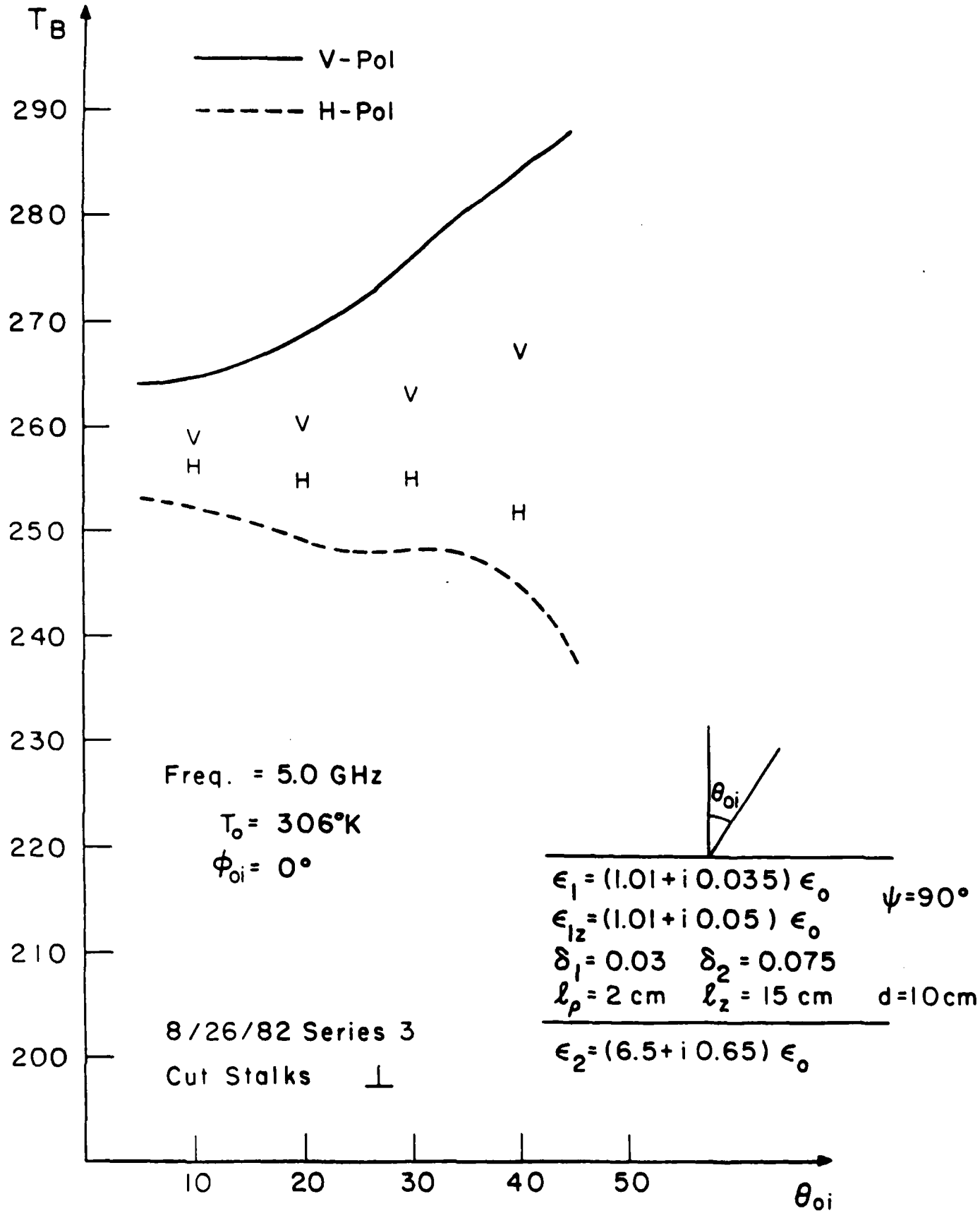
T_B
V-Pol
H-Pol
290
280
270
260
250
240
230
220
210
200
V
V
V
V
H
H
H
H
Freq. = 5.0 GHz
T_o = 306°K
ϕ_{oi} = 0°
8/26/82 Series 3
Cut Stalks ⊥
θ_{oi}
$\epsilon_1 = (1.01 + i\,0.035)\,\epsilon_o$
$\epsilon_{1z} = (1.01 + i\,0.05)\,\epsilon_o$
$\delta_1 = 0.03$ $\delta_2 = 0.075$
$\ell_\rho = 2$ cm $\ell_z = 15$ cm
$\epsilon_2 = (6.5 + i\,0.65)\,\epsilon_o$
ψ=90°
d=10cm
10
20
30
40
50
θ_{oi}

Figure 10

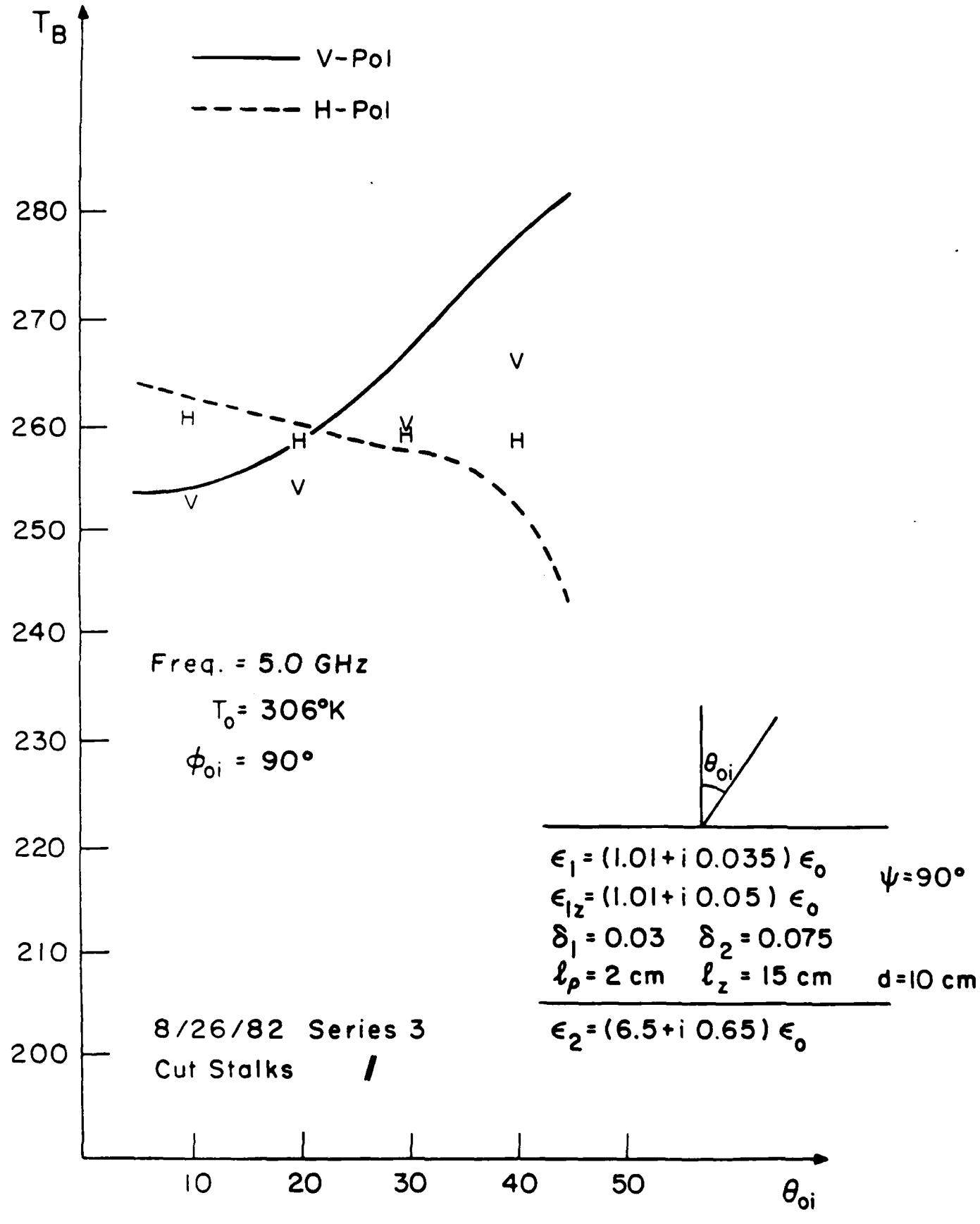
T_B
V-Pol
H-Pol
280
270
260
250
240
230
220
210
200
H
V
V
H
V
H
H
V
Freq. = 5.0 GHz
T_o = 306°K
ϕ_{oi} = 90°
θ_{oi}
$\epsilon_1 = (1.01 + i\,0.035)\,\epsilon_o$
$\epsilon_{1z} = (1.01 + i\,0.05)\,\epsilon_o$
ψ=90°
$\delta_1 = 0.03$ $\delta_2 = 0.075$
ℓ_ρ = 2 cm ℓ_z = 15 cm
d=10 cm
$\epsilon_2 = (6.5 + i\,0.65)\,\epsilon_o$
8/26/82 Series 3
Cut Stalks
10
20
30
40
50
θ_{oi}

DISTRIBUTION LIST

	DODAAD Code	
Leader, Artic, Atmospheric and Ionospheric Sciences Division Office of Naval Research 800 North Quincy Street Arlington, Virginia 22217	N00014	(1)
Administrative Contracting Officer ONRRR - E19-628 Massachusetts Institute of Technology Cambridge, Massachusetts 02139	N66017	(1)
Director Naval Research Laboratory Attn: Code 2627 Washington, D.C. 20375	N00173	(6)
Defense Technical Information Center Bldg. 5, Cameron Station Alexandria, Virginia 22314	S47031	(12)

END

FILMED

7-85

DTIC